Dual Harmonic Injection for Reducing the Sub-module Capacitor Voltage Ripples of Hybrid MMC

Jianzhong Xu, *Senior Member, IEEE*, Weicheng Deng, Chenxiang Gao, Feng Lu, Jun Liang, *Senior Member, IEEE*, Chengyong Zhao*, *Senior Member, IEEE*, and Gen Li*, *Member, IEEE*

Abstract—Reducing the capacitor voltage ripples of the half-bridge sub-modules (HBSM) and full-bridge sub-modules (FBSM) in a hybrid modular multilevel converter (MMC) is expected to reduce the capacitance, volume and costs. To address this issue, this paper proposes a dual harmonic injection method which injects the second harmonic circulating current and third order harmonic voltage into the conventional MMC control. Firstly, the mathematical model of the proposed control is established and analyzed. Then, the general strategy of determining the amplitude and phase angle of each injection component is proposed to suppress the fluctuations of the fundamental and double frequency instantaneous power. The proposed strategy can achieve the optimal power fluctuation suppression under various operating conditions, which also has the advantage of reducing the voltage fluctuation difference between HB and FB SMs. The correctness and effectiveness of the proposed strategy are verified in simulations in PSCAD/EMTDC.

Index Terms—Hybrid modular multilevel converter (MMC); second harmonic circulating current; third harmonic voltage; dual harmonic injection; fluctuation suppression.

NOMENCLATURE

Symbols:	Descriptions
U_{dc}	Pole-to-pole dc voltage.
U_{ac}	Amplitude of the AC-side phase voltage.
I_m	Amplitude of the AC-side phase current.
ω	Fundamental angular frequency.
S, P, Q	Three-phase apparent power, real power and reactive power.
u_{ua}, u_{la}	Instantaneous upper and lower arm voltages in phase *a*.
i_{ua}, i_{la}	Instantaneous upper and lower arm currents in phase *a*.
s_{ua}, s_{la}	Instantaneous upper and lower arm power in phase *a*.
u_{ua_inj}, u_{la_inj}	Instantaneous upper and lower arm voltages in phase *a* with injection.
i_{ua_inj}, i_{la_inj}	Instantaneous upper and lower arm currents in phase *a* with injection.
s_{ua_inj}, s_{la_inj}	Instantaneous upper and lower arm power in phase *a* with injection.
I_2	Amplitude of the injected second order harmonic current.
U_3	Amplitude of the injected third order harmonic voltage.
φ	Power factor angle.
φ_2	Phase angle of the injected second order harmonic current.
φ_3	Phase angle of the injected third order harmonic voltage.

I. INTRODUCTION

Modular multilevel converter (MMC) has higher control flexibility, better modular and scalable capability, fewer harmonics and no commutation failure [1]-[2], as compared to the conventional line commutated converter (LCC). Thanks to these advanced features, MMC based high-voltage direct-current (MMC-HVDC) is more suitable for integrating large-scale renewable energy over long distances, e.g. the offshore wind power [3]. However, the capacitor sub-modules (SMs) of an MMC account for 1/2 of its volume and about 1/3 of the capital cost [4]. Moreover, due to the modular and distributed design of the MMC capacitors, the challenges from circulating currents, harmonic losses [5], and energy balance among SMs may affect the reliability of MMCs [6]. Therefore, it is necessary to investigate the strategies of suppressing capacitor voltage fluctuations, which are applicable to various working conditions. The new strategies are supposed to reduce the SM capacitance, which contributes to reducing the capital cost of the HVDC system [7]-[9].

In case of a DC fault in the MMC-HVDC system, the most straightforward solution is to block the MMCs. However, the half-bridge MMC (HB-MMC) cannot clear fault currents due to its freewheeling diodes. MMCs with current blocking capability have some inherent limitations: the system may experience a temporary interruption of the power transmission and transient overvoltage [10]. Recently, the hybrid MMC, which is composed of half-bridge SMs (HBSMs) and full-bridge SMs (FBSMs), becomes popular due to its advanced DC fault ride-through capability [11]. References [12]-[15] present several technical features of hybrid MMCs by boosting the modulation index (the ratio of the peak AC phase voltage to the DC voltage). These include reducing capacitor voltage ripples, more degrees of freedom for control, reducing current stresses of the devices and adapting to extreme weather conditions, etc. Therefore, hybrid MMCs have gained wide attention from both industry and academia.

The mechanism and suppression schemes of HB-MMCs' capacitor voltage fluctuation have been extensively

investigated [16]-[23]. The third harmonic voltage injection on the modulation reference can optimize the DC voltage utilization rate of MMC. The injection quantity of the amplitude and phase angle for minimizing the amplitude of modulation voltage has been discussed in [19]. The mathematical model of capacitor voltage fluctuation and the second harmonic current injection have been proposed in [20] to reveal the relationship between capacitor voltage and SM power fluctuation. This method aims at eliminating the double-frequency component of the arm instantaneous power, and further reducing the capacitor voltage ripples. Reference [21] proposes a hybrid injection strategy considering both the second harmonic current [20] and the third harmonic voltage [19]. It also evaluates the suppression effects of the capacitor voltage ripples. However, this strategy does not consider the coupling interaction effect of the two types of injections.

For the hybrid MMC with the boosted modulation index, reference [24] proposes an optimal strategy for second harmonic current injection combined with a specific modulation index $m=1.15$. This strategy can suppress both the fundamental frequency component of the arm instantaneous power and the capacitor voltage ripples. In [25], the third harmonic injection modulation [19] and the conventional sinusoidal modulation are applied to the HBSM and FBSM segments of the hybrid MMC. Moreover, the second harmonic current [20] with $m=1.15$ is injected. Although the strategies from [24] and [25] are applied in hybrid MMCs, their harmonic injection method and calculation principle are similar to [21]. Therefore, [21] is selected as the comparison reference, which is defined as a "classical injection method" in this paper. However, the classical scheme is designed with $m=1.15$, thus further optimization is limited by this specific operating condition. In addition, although different mechanisms of the capacitor voltage fluctuations in HBSMs and FBSMs of hybrid MMC are analyzed in [26], the suppression strategies are not discussed, which may have a large impact on the overall capacitor voltage fluctuations [27].

Since the above research does not consider the coupling effect of simultaneous injection when determining the injection phase angles and magnitudes of the second and third order harmonics, the ability of dual harmonic injection to minimize the SM capacitor voltage fluctuation has not been fully utilized. Meanwhile, the optimization strategy in hybrid MMC is used with the modulation index $m=1.15$. However, the effectiveness of the optimized strategy might be reduced under other modulation indexes. To address this issue, an optimal dual harmonic injection method for hybrid MMCs is proposed. The coupling injection effect of second order harmonic circulating current and third order harmonic voltage has been considered to determine the final injection values. The proposed dual harmonic injection can further reduce the overall voltage fluctuation of SM capacitors under different modulation indexes. With the proposed injection method, differences in the voltage fluctuations of HB and FB SMs in the hybrid MMC can be significantly reduced.

II. MATHEMATICAL MODEL OF HARMONIC INJECTION IN HYBRID MMCS

The topology of the hybrid MMC is shown in Fig. 1. Each arm consists of N SMs, including H HBSMs and F FBSMs. U_{dc} and U_{ac} are the amplitudes of DC and AC voltages, I_{dc} and I_m the amplitudes of DC and AC currents, φ the initial phase angle, u_a, u_b and u_c the AC phase voltages, L_{arm} the arm inductor and i_{uj} and i_{dj} the currents of the upper and lower arms of each phase, where $j=a, b, c$.

Fig. 1. Topology of the hybrid MMC.

Phase a is taken as an example considering the three AC phases symmetrical. According to the positive direction identified in Fig. 1, the upper and lower arm voltages u_{ua} and u_{la} are:

$$\begin{cases} u_{ua} = \dfrac{1}{2}U_{dc} - U_{ac}\sin\omega t \\ u_{la} = \dfrac{1}{2}U_{dc} + U_{ac}\sin\omega t \end{cases}, \quad (1)$$

where ω is the fundamental angular frequency.

Ignoring the high-order circulating current components, the upper and lower arm currents are:

$$\begin{cases} i_{ua} = \dfrac{1}{3}I_{dc} + \dfrac{1}{2}I_m\sin(\omega t - \varphi) \\ i_{la} = \dfrac{1}{3}I_{dc} - \dfrac{1}{2}I_m\sin(\omega t - \varphi) \end{cases}. \quad (2)$$

The modulation index m of the hybrid MMC is defined as

$$m = \frac{2U_{ac}}{U_{dc}}. \quad (3)$$

The instantaneous power in the arm is

$$\begin{cases} P_{ua} = U_{ua} \times i_{ua} \\ P_{la} = U_{la} \times i_{la} \end{cases}. \quad (4)$$

Substituting (1) and (2) into (4), the power in the upper and lower arms becomes:

$$\begin{cases} s_{ua} = \dfrac{U_{dc}I_m}{4}\sin\left(\omega t - \varphi\right) + \dfrac{mU_{dc}I_m}{8}\cos\left(2\omega t - \varphi\right) \\ \quad - \dfrac{mU_{dc}I_{dc}}{6}\sin\omega t + \dfrac{U_{dc}I_{dc}}{6} - \dfrac{mU_{dc}I_m}{8}\cos\varphi \\ s_{la} = -\dfrac{U_{dc}I_m}{4}\sin\left(\omega t - \varphi\right) + \dfrac{mU_{dc}I_m}{8}\cos\left(2\omega t - \varphi\right) \\ \quad - \dfrac{mU_{dc}I_{dc}}{6}\sin\omega t + \dfrac{U_{dc}I_{dc}}{6} + \dfrac{mU_{dc}I_m}{8}\cos\varphi \end{cases} \quad (5)$$

In steady-state, there is no DC power component in the arms. Otherwise, the accumulated energy in capacitors will increase or decrease continuously. Therefore, the DC component in equation (5) should be zero. Then, $I_{dc} = \dfrac{3}{4}mI_m\cos\varphi$ can be obtained. Equation (5) can be simplified to:

$$\begin{cases} s_{ua} = \dfrac{U_{dc}I_m}{4}\sin\left(\omega t - \varphi\right) - \dfrac{m^2 U_{dc}I_m}{8}\cos\varphi\sin\omega t \\ \quad + \dfrac{mU_{dc}I_m}{8}\cos\left(2\omega t - \varphi\right) \\ s_{la} = -\dfrac{U_{dc}I_m}{4}\sin\left(\omega t - \varphi\right) + \dfrac{m^2 U_{dc}I_m}{8}\cos\varphi\sin\omega t \\ \quad + \dfrac{mU_{dc}I_m}{8}\cos\left(2\omega t - \varphi\right) \end{cases} \quad (6)$$

The second harmonic circulating current injection strategy is implemented by controlling the amplitude and phase angle of the second harmonic circulating component to the set value [20]. The amplitude is I_2 and the phase angle is φ_2. Ignoring the higher-order harmonic component [20], the upper and lower arm currents are:

$$\begin{cases} i_{ua\_inj} = \dfrac{1}{3}I_{dc} + \dfrac{1}{2}I_m\sin\left(\omega t - \varphi\right) + I_2\sin(2\omega t + \varphi_2) \\ i_{la\_inj} = \dfrac{1}{3}I_{dc} - \dfrac{1}{2}I_m\sin\left(\omega t - \varphi\right) + I_2\sin(2\omega t + \varphi_2) \end{cases} \quad (7)$$

The third harmonic voltage injection scheme refers to superimposing the third harmonic zero-sequence component on the three-phase modulation waves [19]. The amplitude and phase angle of the injected voltage are set as U_3 and φ_3. The voltages of the upper and lower arms are expressed as:

$$\begin{cases} u_{ua\_inj} = \dfrac{1}{2}U_{dc} - U_{ac}\sin\left(\omega t\right) - U_3\sin(3\omega t + \varphi_3) - u_{cir} \\ u_{la\_inj} = \dfrac{1}{2}U_{dc} + U_{ac}\sin\left(\omega t\right) + U_3\sin(3\omega t + \varphi_3) - u_{cir} \end{cases} \quad (8)$$

In equation (8), u_{cir} is the second order voltage component generated by controlling the second order harmonic circulating current. u_{cir} is usually ignored in the control system when analyzing the capacitor voltage fluctuations since its magnitude is small [21],[24],[26],[27]. To simplify the presentation, the second and third harmonic injection coefficients k_2 and k_3 are defined as (the subscripts 2 and 3 indicate the second and third harmonics):

$$\begin{cases} k_2 = \dfrac{3I_2}{I_{dc}} \\ k_3 = \dfrac{2U_3}{U_{dc}} \end{cases} \quad (9)$$

Combining (7), (8) and (9), the voltage and current of the arm with the second and third harmonic injections are obtained as follows:

$$\begin{cases} u_{ua\_inj} = \dfrac{1}{2}U_{dc}\left(1 - m\sin\left(\omega t\right) - k_3\sin(3\omega t + \varphi_3)\right) \\ i_{ua\_inj} = \dfrac{1}{3}I_{dc}(1 + \dfrac{2}{m\cos\varphi}\sin\left(\omega t - \varphi\right) + k_2\sin(2\omega t + \varphi_2)) \end{cases} \quad (10)$$

Therefore, the instantaneous power of the arm can be expressed as

$$s_{ua\_inj} = \sum_{i=0}^{n} s_{ua\_inj\_i}, \quad (11)$$

where $s_{ua\_inj\_i}$ represents the i-th order frequency component of the arm instantaneous power and n represents the number of harmonics. According to equation (8), each component can be derived as:

$$\begin{bmatrix} s_{ua\_inj\_0} \\ s_{ua\_inj\_1} \\ s_{ua\_inj\_2} \\ s_{ua\_inj\_3} \\ s_{ua\_inj\_4} \\ s_{ua\_inj\_5} \end{bmatrix} = \dfrac{I_{dc}U_{dc}}{6m\cos\varphi}\begin{bmatrix} 0 \\ \frac{1}{2}\begin{bmatrix} -k_2k_3m\cos\varphi\cos(\omega t - \varphi_2 + \varphi_3) - k_2 m^2\cos\varphi\cos(\omega t + \varphi_2) \\ -2m^2\sin(\omega t)\cos\varphi + 4\sin(\omega t - \varphi) \end{bmatrix} \\ \begin{bmatrix} k_2 m\cos\varphi\sin(2\omega t + \varphi_2) - k_3\cos(2\omega t + \varphi + \varphi_3) \\ + m\cos(2\omega t - \varphi) \end{bmatrix} \\ \frac{1}{2}m\left[-2k_3\sin(3\omega t + \varphi_3)\cos\varphi + mk_2\cos\varphi\cos(3\omega t + \varphi_2)\right] \\ k_3\cos(4\omega t - \varphi + \varphi_3) \\ \frac{1}{2}mk_2k_3\cos\varphi\cos(5\omega t + \varphi_2 + \varphi_3) \end{bmatrix}. \quad (12)$$

The detailed derivation of Equation (12) is shown in the appendix. Equation (12) shows the mathematical expressions of the fundamental and low-order harmonics of the arm power, which can be used to derive the conditions of the second and third harmonic injection coefficients k_2 and k_3 of the proposed strategy.

III. PROPOSED DUAL HARMONIC INJECTION STRATEGY

The range of the capacitor voltage ripples is positively correlated with that of the arm power fluctuation [20]. Therefore, suppressing the fundamental frequency component and the second harmonic component of the arm power can effectively reduce capacitor voltage ripple. This section proposes a general strategy of optimally injecting the second harmonic circulating current and third harmonic voltage to the modulation reference of hybrid MMCs, so as to suppress the fundamental and second frequency components of the arm power. This is the main contribution of this paper.

A. General fluctuation suppression strategy of the fundamental-frequency component

From equation (12), the fundamental-frequency component fluctuation of the arm instantaneous power is obtained:

$$s_{ua\_inj\_1} = \dfrac{I_{dc}U_{dc}}{12m\cos\varphi}\begin{bmatrix} -k_2k_3m\cos\varphi\cos(\omega t - \varphi_2 + \varphi_3) - k_2 m^2\cos\varphi\cos(\omega t + \varphi_2) \\ -2m^2\sin(\omega t)\cos\varphi + 4\sin(\omega t - \varphi) \end{bmatrix}. \quad (13)$$

From the trigonometric identity transformation of equation (13), the fundamental power $s_{ua\_inj\_1}$ can be expressed as two orthogonal quantities:

$$s_{ua\_inj\_1} = A_1 \cos(\omega t) + B_1 \sin(\omega t), \tag{14}$$

where A_1 and B_1 are:

$$\begin{cases} A_1 = \dfrac{I_{dc}U_{dc}}{12m\cos\varphi}(-4\sin\varphi - k_2 m^2 \cos\varphi\cos\varphi_2 \\ \qquad -k_2 k_3 m\cos\varphi\cos(\varphi_2 - \varphi_3)) \\ B_1 = \dfrac{I_{dc}U_{dc}}{12m\cos\varphi}(-2m^2\cos\varphi + 4\cos\varphi + \\ \qquad k_2 m^2 \cos\varphi\sin\varphi_2 + k_2 k_3 m\cos\varphi\sin(\varphi_3 - \varphi_2)) \end{cases} \tag{15}$$

Let $A_1=B_1=0$ to suppress the fundamental-frequency component fluctuation of the power. Moreover, k_2, k_3, φ_2 and φ_3 should satisfy the following formulas

$$\begin{cases} k_2 = f_1(\varphi_2, \varphi_3) \\ k_3 = f_2(\varphi_2, \varphi_3) \end{cases}, \tag{16}$$

where the functions f_1 and f_2 are defined as follows

$$\begin{cases} f_1(\varphi_2,\varphi_3) = \dfrac{-4\cos(\varphi_3 - \varphi_2 + \varphi) + 2m^2\cos\varphi\cos(\varphi_3 - \varphi_2)}{m^2\cos\varphi\sin(2\varphi_2 - \varphi_3)} \\ f_2(\varphi_2,\varphi_3) = \dfrac{(-m^3 + 2m)\cos\varphi\cos\varphi_2 - 2m\sin\varphi\sin\varphi_2}{m^2\cos\varphi\cos(\varphi_3 - \varphi_2) - 2\cos(\varphi_3 - \varphi_2 + \varphi)} \end{cases} \tag{17}$$

The second and third harmonic injection coefficient k_2 and k_3 can be obtained by solving equations (16) and (17) when the power factor φ and modulation index m are given. Then, the optimal suppression of fundamental-frequency fluctuation can be obtained. As the above suppression strategy can under various modulation indexes and power factor conditions, it can be considered as a general injection strategy for fundamental components.

B. General fluctuation suppression strategy of the double-frequency component

According to equation (12), the double-frequency fluctuation of the arm instantaneous power can be obtained

$$s_{ua\_inj\_2} = \dfrac{I_{dc}U_{dc}}{6m\cos\varphi}\begin{bmatrix} -k_3\cos(2\omega t + \varphi + \varphi_3) + m\cos(2\omega t - \varphi) \\ +k_2 m\cos\varphi\sin(2\omega t + \varphi_2) \end{bmatrix}. \tag{18}$$

From the trigonometric identity transformation of equation (18), the second harmonic power $s_{ua\_inj\_2}$ can be expressed as two orthogonal quantities:

$$s_{ua\_inj\_2} = A_2\cos(2\omega t) + B_2\sin(2\omega t), \tag{19}$$

where A_2 and B_2 are

$$\begin{cases} A_2 = \dfrac{I_{dc}U_{dc}}{6m\cos\varphi}(k_2 m\cos\varphi\sin\varphi_2 - k_3\cos(\varphi_3 + \varphi) + m\cos\varphi) \\ B_2 = \dfrac{I_{dc}U_{dc}}{6m\cos\varphi}(k_2 m\cos\varphi\cos\varphi_2 + k_3\sin(\varphi_3 + \varphi) + m\sin\varphi) \end{cases} \tag{20}$$

Let $A_2=B_2=0$ to eliminate the double-frequency component fluctuation of the power. Moreover, k_2, k_3, φ_2 and φ_3 should satisfy the following formulas

$$\begin{cases} k_2 = f_3(\varphi_2, \varphi_3) \\ k_3 = f_4(\varphi_2, \varphi_3) \end{cases}, \tag{21}$$

where the functions of f_3 and f_4 are defined as follows

$$\begin{cases} f_3(\varphi_2,\varphi_3) = \dfrac{-\sin(\varphi_3 + 2\varphi)}{\cos\varphi\sin(\varphi_3 + \varphi - \varphi_2)} \\ f_4(\varphi_2,\varphi_3) = \dfrac{m\cos(\varphi_2 + \varphi)}{\cos(\varphi_3 + \varphi - \varphi_2)} \end{cases}. \tag{22}$$

The second and third harmonic injection coefficient k_2 and k_3 can be obtained by solving equations (21) and (22) when the power factor φ and modulation index m are given. Then, the optimal suppression of double-frequency fluctuation can be obtained. Similar to the above injection strategy for the fundamental-frequency component, the injection strategy for second order harmonic component fluctuation is also applicable to various modulation indexes and power factor conditions.

C. Amplitude constraints of the injected harmonics

Considering the normal operating conditions and the electrical stress of the devices, the injection of the second and third harmonics must be properly designed.

With respect to the second harmonic current injection, the amplitude of the second harmonic current injection k_{2t} in the classical injection method [21] is defined as:

$$k_{2t} = \dfrac{3mI_m}{4I_{dc}}. \tag{23}$$

In order to avoid increasing the electrical stress, the final second harmonic circulating injection coefficient k_2 should satisfy

$$|k_2| \le |k_{2t}|. \tag{24}$$

As for the third harmonic voltage injection, when it is not activated, the negative peak value of the arm reference voltage U_{ua_min} can be calculated by

$$U_{ua\_min} = \dfrac{1}{2}U_{dc}(1-m). \tag{25}$$

With the third harmonic voltage injection, the negative peak value of $U_{ua\_inj\_min}$ becomes:

$$U_{ua\_inj\_min} = \min u_{ua\_inj}. \tag{26}$$

The hybrid MMC control strategy can automatically determine that the arm reference voltage is only supported by FBSMs when the arm voltage is negative. This is a pre-set process. Therefore, the negative peak $U_{ua\_inj\_min}$ with the third harmonic voltage injection should not exceed the negative peak of U_{ua_min}. Thus, the third harmonic voltage injection coefficient k_3 should satisfy equation (27), which is calculated from equations (8) and (26):

$$k_3 \leq -\frac{m}{3} + \mathrm{Re}\left[\frac{\left(\frac{2}{3}\right)^{1/3} m^2}{\left(-3m^3 + i\sqrt{3}m^3\right)^{1/3}} + \frac{\left(-3m^3 + i\sqrt{3}m^3\right)^{1/3}}{2^{1/3}3^{2/3}} \right]. \quad (27)$$

Then the amplitudes of the second and third harmonic injections can be determined according to equations (24) and (27).

D. General calculation method of the final references under the dual harmonic injection

To reduce the capacitor voltage ripples of both HBSMs and FBSMs in hybrid MMCs, according to equations (17) and (22), the following optimal injection can be obtained when equation (28) is satisfied.

$$\begin{cases} f_1\left(\varphi_2, \varphi_3\right) = f_3\left(\varphi_2, \varphi_3\right) \\ f_2\left(\varphi_2, \varphi_3\right) = f_4\left(\varphi_2, \varphi_3\right) \end{cases}. \quad (28)$$

Considering the constraint equations (24) and (27), the results from (28) are shown in Fig. 2. Considering the practical engineering application, m will not be too low in normal operation, generally around 1. Therefore, the range of m is (0.8-1.4) after considering the margin. Area1 and area2 are obtained from equation (28). It can be seen that the results vary with the change of m and $\cos \varphi$. In area1, the fundamental and double frequency fluctuations of the power can be eliminated. In area2, where the modulation index is relatively small and the power factor is close to zero, the goal of the simultaneous suppression cannot be achieved. In this area, equation (16) is satisfied, which indicates that the fundamental frequency power fluctuations can be suppressed. However, this is not the case for equation (21).
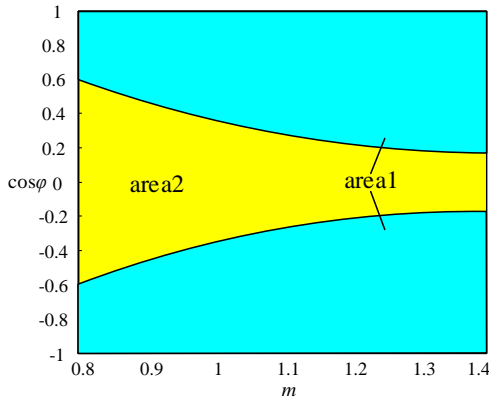

Fig. 2. Solutions for fundamental and double frequency power suppression.

Therefore, under the constraint of (16), there should be an optimal injection combination that can suppress the double-frequency component fluctuations as much as possible. From equations (19) and (20), the amplitude of the second harmonic power $s_{\text{ua\_inj\_2}}$ can be obtained. Therefore, the objective function can be defined as:

$$\min F(\varphi_2, \varphi_3) = \left| S_{ua\_inj\_2} \right|^2 = k_3^2 + (1 + k_2^2 \cos\varphi^2)m^2 -$$
$$2m[k_3 \cos(\varphi_3 + 2\varphi) - k_2 m \cos\varphi \sin(\varphi_2 + \varphi) - k_3 k_2 \cos\varphi \sin(\varphi_3 - \varphi_2 + \varphi)] . \quad (29)$$
$$s.t.$$
$$\begin{cases} k_2 = f_1(\varphi_2, \varphi_3) \\ k_3 = f_2(\varphi_2, \varphi_3) \end{cases}$$

The objective function is to minimize the amplitude of the second harmonic power $s_{\text{ua\_inj\_2}}$.

Fig. 3 shows the flow chart of optimizing area2. Supposing φ_2, $\varphi_3 \in [-\pi, \pi]$, φ_{20} and φ_{30} are the initial values of the phase angle of the second and third harmonic injections ($\varphi_{20}=\varphi_{30}=-\pi$). Meanwhile, d_2 and d_3 are the changing steps of the phase angles. For each group of (φ_2, φ_3), φ_2 and φ_3 are substituted into equation (16) to calculate k_2 and k_3. This will ensure a complete suppression of the fundamental-frequency power fluctuation. If the constraint equations (24) and (27) are satisfied, (φ_2, φ_3, k_2, k_3) will be substituted into equation (29) to obtain the value of objective function $\min F(\varphi_2, \varphi_3)$, and record them as a group (φ_2, φ_3, $F(\varphi_2, \varphi_3)$). Then the values of φ_2 and φ_3 are changed and the above process is repeated until φ_2 and φ_3 reach the maximum (π). Finally, the combination of (φ_{2op}, φ_{3op}) will be determined to minimize the ripples of the double-frequency component.
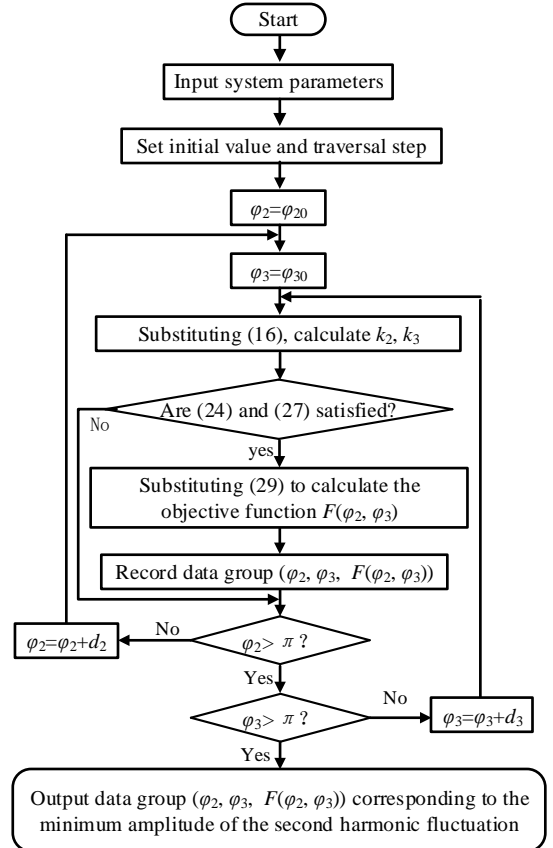

Fig. 3. Flow chart of calculating the optimal injection in area2.

The implementation of the proposed dual harmonic injection method is shown in Fig. 4. Δu_2 and Δu_3 refer to correction voltages of the second and third order harmonic injections. e_{j_ref} represents the modulation reference in j-phase from the conventional MMC dq-frame control. Firstly, the area of working conditions (m, $\cos \varphi$) should be determined. If (m, $\cos \varphi$) falls into area1, solving (28) will achieve the suppression of

fundamental and double frequency fluctuations. Otherwise, if (m, cos φ) falls into area2, the optimization process in Fig. 3 will be activated to minimize the overall capacitor voltage fluctuations. Further, the optimized injection group ($k2$, $k3$, $\varphi2$, $\varphi3$), which is pre-calculated offline, is set as the reference of the harmonic generator, as shown in Fig. 4. Then, the harmonic voltage generator outputs the voltage correction Δu_2 and Δu_3 which will be superimposed on the modulation waves. Finally, the reference value of arm voltage for modulation is obtained.
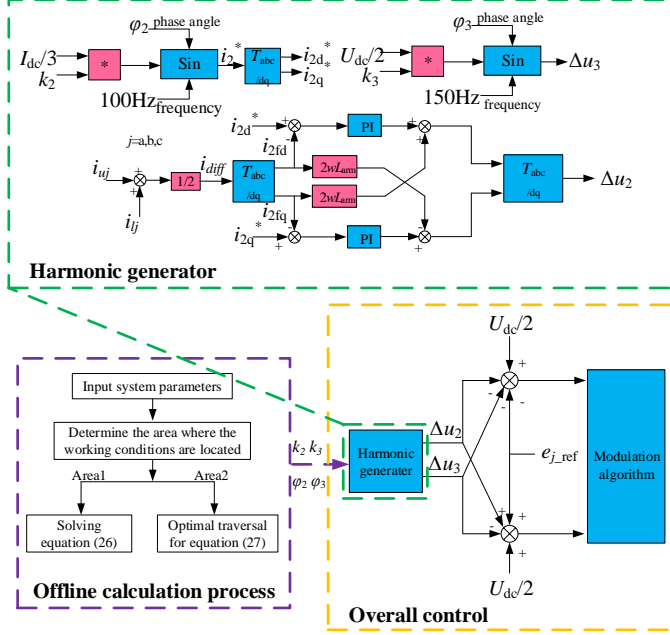

Fig. 4. Control blocks of the proposed control method.

To compare the proposed control strategy with the injection strategy reported in [21], the power fluctuation amplitudes obtained from both methods are plotted in Fig. 5. The parameters in Table I are used for both strategies.

TABLE I
PARAMETERS OF THE TEST SYSTEM

Items/Unit	Values
AC side voltage / kV	168/176/184/192/200
Modulation index	1.05/1.1/1.15/1.2/1.25
DC voltage / kV	320
Rated power / MW	500
Capacitance of SM / µF	10000
Number of FBSMs	130
Number of HBSMs	100
Arm reactor / H	0.06
Capacitor voltage reference / kV	1.39

As shown in Fig. 5, the arm instantaneous power fluctuation peak values form the surface S_2 in case of using the proposed strategy. S_2 is lower than the surface S_1 obtained from the method reported in [21]. The voltage ripples can also be effectively reduced in the proposed control strategy since the capacitor voltage fluctuations are similar to the power fluctuations.
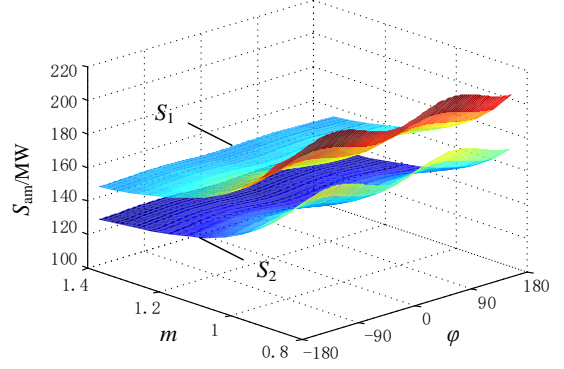

Fig. 5. Comparison of power fluctuation amplitudes.

IV. SUPPRESSION EFFECTS OF THE VOLTAGE FLUCTUATION DIFFERENCE BETWEEN HBSMs AND FBSMs

Under the boosted modulation of hybrid MMCs, there are negative periods of the arm reference voltage, as shown in Fig. 6. During this period, only the FBSMs participate in the sorting algorithm. Therefore, FBSMs will be charged and discharged more frequently than HBSMs, arising from the difference in capacitor voltage fluctuations between the two types of SMs [26]-[27].
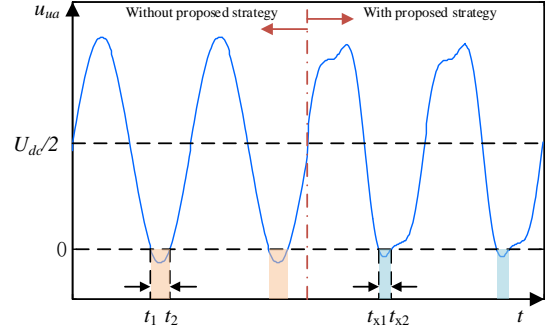

Fig. 6. The arm reference voltage of hybrid MMC.

Simulations have shown that the energy accumulation of FBSMs during the above period is positively correlated with the range of the fluctuation difference. To conduct a quantitative comparison, the proposed control strategy is not activated initially. During the period (t_1, t_2), the average energy accumulation ΔE_F of FBSMs is:

$$\Delta E_F = \frac{1}{F}\left|\int_{t_1}^{t_2} s_{ua}dt\right|, \tag{30}$$

where F is the number of FBSMs. When the proposed control is triggered, the period of the negative voltage is reduced to (t_{x1}, t_{x2}), as shown in Fig. 6. Then the arm power is suppressed to S_{ua_inj} instead of S_{ua}, and equation (30) will be updated to:

$$\Delta E_{F1} = \frac{1}{F}\left|\int_{t_{x1}}^{t_{x2}} s_{ua\_inj}dt\right|. \tag{31}$$

It is found that the negative interval of the arm reference voltage is reduced due to the application of the proposed control strategy. The instantaneous power fluctuation of the arm is reduced as well since the fundamental and double

frequency components of the instantaneous power of the arm are suppressed. Based on the previous equations of arm power, the following relationship can be proved:

$$\left|\Delta E_{\mathrm{F1}}\right| < \left|\Delta E_{\mathrm{F}}\right|. \tag{32}$$

In this paper, the proposed control is not intentionally designed to reduce the voltage difference between two types of SMs in hybrid MMCs. However, thanks to the reduced capacitor voltage fluctuations, the switching of FB and HB SMs is improved with more balanced SM voltages, which is an additional benefit of the proposed control.

V. VERIFICATION AND ANALYSIS

In this section, a point-to-point hybrid MMC-HVDC link is simulated in PSCAD/EMTDC to verify the proposed control strategy. System parameters are given in Table I. In this system, one station regulates the DC voltage and the other controls the power. The proposed control is applied in the Vdc controlling station to verify its effectiveness.

A. Verification of the steady-state operation

The HVDC system reaches the steady-state at time t=3.0s with m=1.25 and $\cos\varphi$=1. At time t=4.0s, the proposed control strategy is activated. The AC voltages, arm reference voltage, capacitor voltage ripple and arm current are shown in Fig. 7.
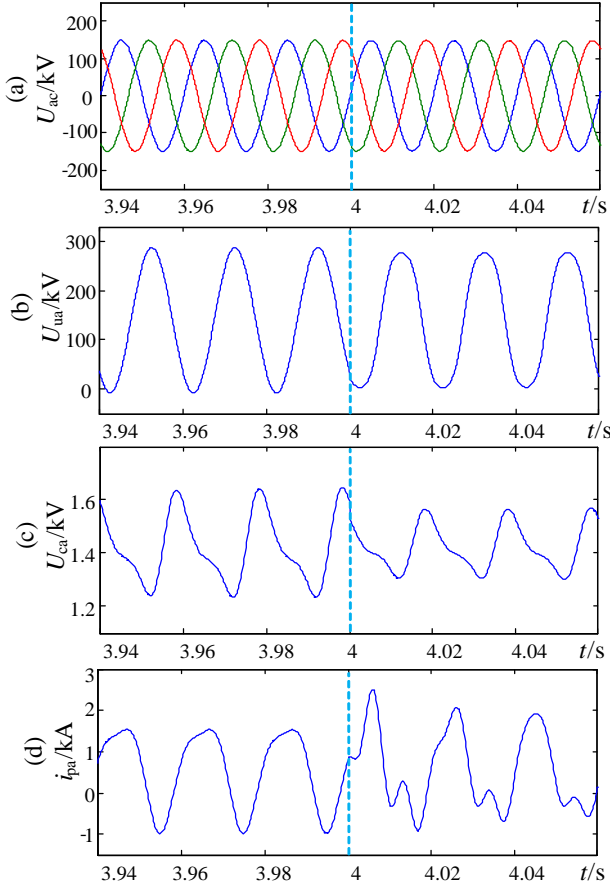

Fig. 7 Steady-state waveforms of the hybrid MMC: (a) AC voltages; (b) reference voltage of arm; (c) capacitor voltage ripples; (d) arm current.

Fig. 7 shows that the proposed control does not affect the normal operation of the HVDC system and can reduce the amplitudes of the capacitor voltage ripples by suppressing the power fluctuations.

B. Verification of the overall fluctuation suppression and capacitance reduction effects

Fig. 8 shows the peak-peak results of the overall fluctuations of the capacitor voltage $U_{\mathrm{p\text{-}p}}$, with the proposed injection strategy, the classical injection strategy, and without using any additional injection strategy under various operating conditions.
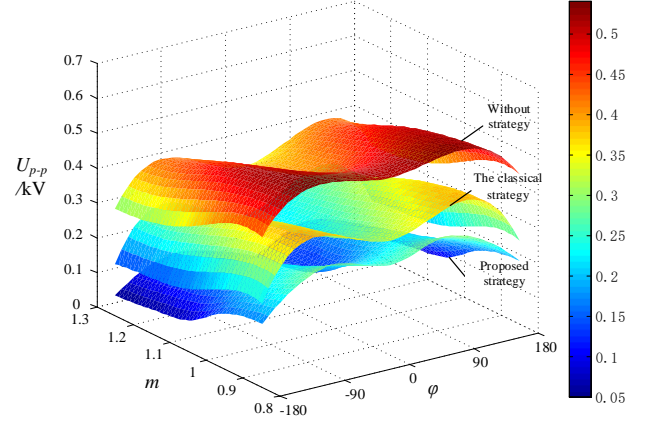

Fig. 8. Comparison of the voltage fluctuations of capacitor voltage $U_{\mathrm{p\text{-}p}}$.

Fig. 8 illustrates that the proposed strategy can largely reduce the peak-peak value of the overall capacitor voltage fluctuations compared with the classical injection strategy and systems without additional control strategy. For a larger m, this percentage can be further increased.

Given a specific ripple limit, the proposed strategy has the minimum requirement of the SM capacitor. In order to evaluate the relationship more accurately, the following calculation can be made. Assuming the ratios of the positive and negative peak values of the overall capacitor voltages to the rated value are η_1 and η_2, which satisfy:

$$\begin{cases} U_{C,\min} = U_C\left(1-\eta_2\right) \\ U_{C,\max} = U_C\left(1+\eta_1\right) \end{cases}. \tag{33}$$

where $U_{C,\min}$ and $U_{C,\max}$ are the positive and negative peak values of the capacitor voltages and U_C is the rated value. During the whole cycle, the maximum stored energy ΔW_{SM} of each capacitor can be expressed as:

$$\Delta W_{SM} = \frac{1}{2} C_0 \left(U_{C,\max}^2 - U_{C,\min}^2\right). \tag{34}$$

Taking the upper arm in phase a as an example. Let ε be any time within $(0, T)$. Then, the integral of the arm power within $(0, \varepsilon)$ is W_{ua}:

$$W_{ua}(m) = \int_0^\varepsilon p_{ua}\left(\omega t\right)d\left(\omega t\right) \quad \varepsilon \in \left(0, T\right). \tag{35}$$

In one period, the expression of the maximum value of ΔW_{SM} is:

$$\Delta W_{SM}(m) = \frac{1}{N}\left(\max W_{ua}(m) - \min W_{ua}(m)\right). \tag{36}$$

According to equations (34) and (36), the SM capacitance C_0 can be obtained:

$$C_0 = \frac{2S}{3mN\omega U_C^2\left[(1+\eta_1)^2-(1-\eta_2)^2\right]}\left[1-\left(\frac{m\cos\varphi}{2}\right)^2\right]^{\frac{3}{2}}. \quad (37)$$

where N is the number of SMs per arm. Assuming the transmitted power of the converter is constant, the capacitance variation is ΔC, and the corresponding variations of η_1 and η_2 are $\Delta\eta_1$ and $\Delta\eta_2$. Therefore, from (37), the mathematical relationship between ΔC and $\Delta\eta_1$ and $\Delta\eta_2$ is as

$$C_0 + \Delta C = \frac{2S}{3mN\omega U_C^2\left[(1+\eta_1+\Delta\eta_1)^2-(\eta_2+\Delta\eta_2-1)^2\right]}.$$
$$\left[1-\left(\frac{m\cos\varphi}{2}\right)^2\right]^{\frac{3}{2}} \quad (38)$$

Substituting (37) into (38), the capacitance variation ΔC can be obtained:

$$\Delta C = \left[\frac{\Delta\eta_1^2-\Delta\eta_2^2+2(1+\eta_1)\Delta\eta_1+2(1-\eta_2)\Delta\eta_2}{\left[(1+\eta_1)^2-(1-\eta_2)^2\right]\left[(1+\eta_1+\Delta\eta_1)^2-(\eta_2+\Delta\eta_2-1)^2\right]}\right].$$
$$\frac{2S}{3mN\omega U_C^2}\left[1-\left(\frac{m\cos\varphi}{2}\right)^2\right]^{\frac{3}{2}} \quad (39)$$

Using equation (39), two operating conditions are calculated: condition 1 (m=1.05, cos φ=1); condition 2 (m=1.25, cos φ=1). The capacitance reduction results are given in Table II.

TABLE II
COMPARISON OF SM CAPACITANCE VALUE REDUCTION

Operating conditions	Capacitance reduction ratio	
	Classical strategy	Proposed strategy
1	18.5%	27.5%
2	29.2%	43.4%

It can be seen from Table II that the proposed control can further reduce the capacitance requirements of hybrid MMCs compare to the classical control. This, in turn, proves the effectiveness of the proposed dual harmonic injection strategy.

In addition, the proposed strategy is capable to reduce the capacitance by 40%. In case of m=1.25, the average module voltages of a standard capacitance of 10000 μF (without the proposed scheme) and a reduced capacitance of 6000 μF (with the proposed scheme) are shown in Fig. 9. It can be observed that the proposed strategy can largely reduce the capacitance without sacrificing the fluctuation of the average module voltage (less than 1.4 % higher).
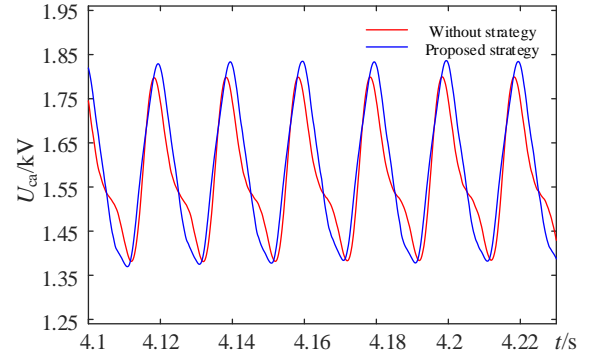

Fig. 9 Average module voltages with standard and reduced capacitor values.

C. Verification of the voltage ripples under dynamic changes

At t=5.0s, the power setpoint is respectively step changed with a 10% increase and 10% decrease. The averaged capacitor voltage fluctuations of HB and FB SMs are shown in Figs. 9(a) and (b).
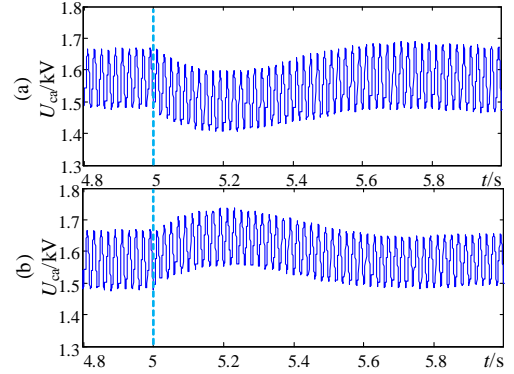

Fig. 9. Dynamic responses of SM voltages. (a) 10% step-up of the real power; (b) 10% step-down of the real power.

Fig. 9 shows that the dynamic responses under the two power step changes are smooth. When the system reaches stable, the peak-peak capacitor voltages in the two cases also reach to new values which are either 10% larger or smaller than their previous values. This is reasonable because the capacitor voltage fluctuation is positively correlated with the transmitted real power of the hybrid MMC.

D. Verification of the voltage balancing of HB and FB SMs

The capacitor voltage ripples of HB and FB SMs are compared under two operating conditions of m=1.05 and m=1.25. The results are shown in Figs. 10(a) and (b). At t=4.0s, the proposed strategy is activated and the overall SM capacitor voltage fluctuations are suppressed. More comparison results with different modulation indexes are shown in Fig. 10(c). U_{dif} refers to the peak-peak value of fluctuation difference between the two types of SMs.
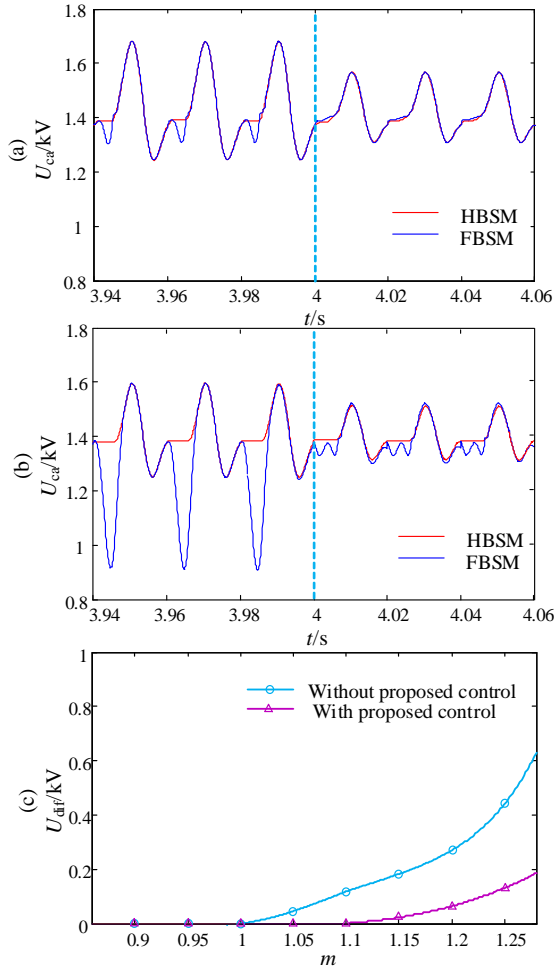
Fig. 10. Comparison of voltage fluctuations between HB and FB SMs: (a) m=1.05, $\cos\varphi$=1; (b) m=1.25, $\cos\varphi$=1; (c) $m\in[0.85,1.3]$, $\cos\varphi$=1.

It is observed that the capacitor voltage fluctuations of HB and FB SMs can be largely reduced once the proposed injection strategy is triggered. Moreover, the voltage difference between the two types of SMs is reduced. As shown in Fig. 10(c), a larger modulation index m leads to a worse voltage difference suppression performance. This is because that the FBSMs are more frequently charged and discharged under a large m. This phenomenon is observed in both two cases with and without the proposed control. However, it can be seen that voltage difference suppression of the proposed control performs better than the case without additional control in any value of m. The results also indicate that the voltage difference of the two types of SMs in a hybrid MMC cannot be completely suppressed under any value of m.

E. Verification of the harmonic spectrum of arm currents

As both the classical and proposed strategies will inject harmonics into each arm of the hybrid MMC, the harmonic spectrum of the arm currents should be carefully evaluated and compared. Fig. 11 shows the harmonics of the arm currents under the aforementioned two operating conditions.
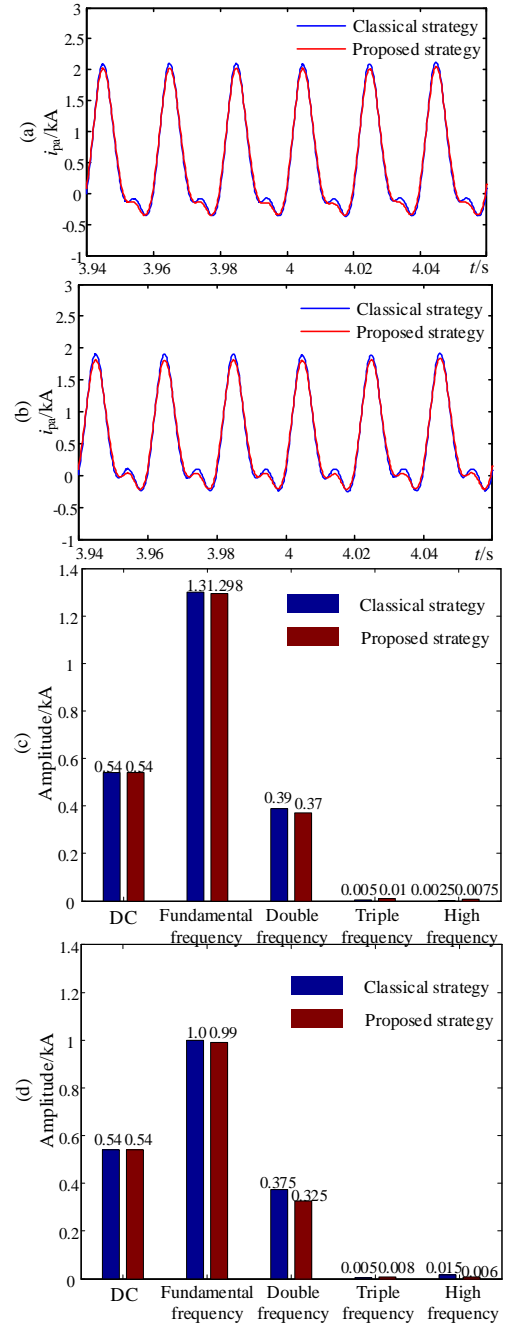

Fig. 11. Comparisons of arm currents: (a) m=1.05, $\cos\varphi$=1; (b) m=1.25, $\cos\varphi$=1; (c) arm current spectrum (m=1.05, $\cos\varphi$=1); (d) arm current spectrum (m=1.25, $\cos\varphi$=1).

It is observed from Figs. 11(a) and (b) that the proposed control strategy does not affect the current profile too much under different operating conditions. Fig. 11(c) shows that the arm current is mainly composed of DC, fundamental and double frequency components. The amplitudes of the third and higher-order frequency components are relatively small. Compared with the classical strategy, under both operating conditions, the fundamental frequency components of the arm current are almost unaffected, and the double frequency components are slightly reduced. Although slight increments are observed in the third and higher-order harmonics, their amplitudes are much smaller than the fundamental and double frequency components. Therefore, the normal operation will

not be affected by the proposed control strategy.

F. Verification of the transient performance

A grid-side single-phase-to-ground fault has been set at $t = 6$ s to test the transient performance of the proposed strategy. The fault resistance is 300 Ω with a duration of 100 ms. The fault leads to a 15% voltage drop in the faulted phase. The behaviors of the capacitor voltages without and with the proposed strategy are shown in Fig. 13.
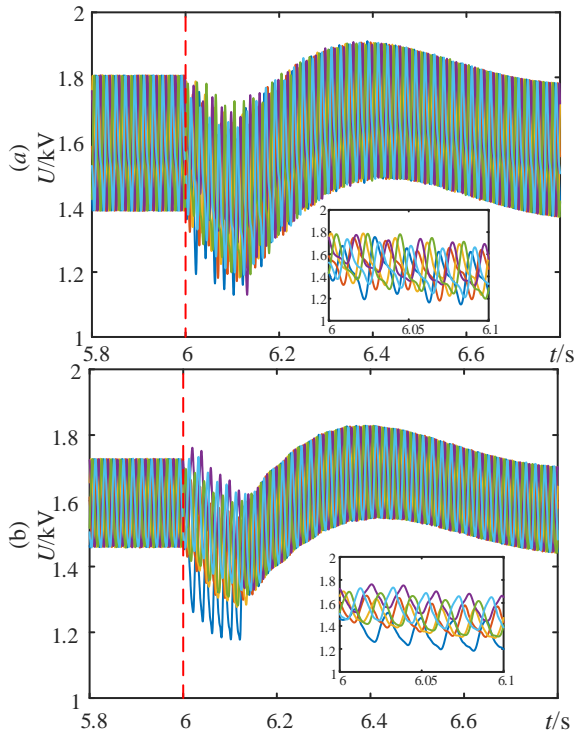

Fig. 13 MMC capacitor voltages under a grid-side single-phase fault. (a) without the proposed strategy; (b) with the proposed strategy.

It can be seen from Fig. 13 that the proposed strategy shows better performance with less capacitor voltage ripples in both steady and transient states compared to the system without using the proposed strategy. Moreover, during the fault, the capacitor voltages experience less distortions in case of using the proposed control strategy. The systems in the two cases recover to steady-state in similar manners. This study shows that the proposed harmonic injection control would not affect the fault tolerant operation of the converters.

VI. CONCLUSIONS

In this paper, a general suppression strategy for sub-module capacitor voltage ripples of hybrid MMC has been proposed using an optimal dual injection of the second harmonic circulating current and third harmonic voltage into the conventional MMC control. With the proposed control strategy, the fundamental and double frequency components of the arm power can be both eliminated and therefore, the capacitor voltage ripples can be significantly reduced at the same time.

The proposed strategy has better performance in reducing the overall fluctuation of the capacitor voltages. The peak-peak capacitor voltage fluctuation of all SMs can be largely reduced.

More importantly, the capacitance of hybrid MMC can be reduced if the proposed control strategy is employed. The difference of the voltage fluctuation between HB and FB SMs is also well suppressed under the proposed control strategy. Simulations and calculations have shown that the proposed strategy has few impacts on the normal operation of the hybrid MMC-HVDC system, in terms of harmonics and losses. It should be also highlighted that the impact of the proposed control strategy on operation under weak grid conditions and reduced capacitor values, although highly desirable to verify its robustness, falls out of the scope of this paper.

REFERENCES

[1] A. Lesnicar and R. Marquardt, "A new modular voltage source inverter topology," in *Proc. EPE*, Toulouse, France, Sep. 2–4, 2003, pp. 1–10.

[2] A. Lesnicar and R. Marquardt, "An innovative modular multilevel con verter topology suitable for a wide power range," in *Proc. IEEE Bologna PowerTech Conf.*, " Bologna, Italy, Jun. 23–26, 2003, pp. 1–6.

[3] S. Debnath, J. Qin, B. Bahrani, M. Saeedifard and P. Barbosa, "Operation, Control, and Applications of the Modular Multilevel Converter: A Review," *IEEE Trans. Power Electron.*, vol. 30, no. 1, pp. 37-53, Jan. 2015.

[4] M. M. C. Merlin and T. C. Green, "Cell capacitor sizing in multilevel converters： cases of the modular multilevel converter and alternate arm converter," *IET Power Electron.*, vol. 8, no. 3, pp. 350-360, Jan. 2015.

[5] M. Guan, Z. Xu, "Modeling and Control of a Modular Multilevel Converter-Based HVDC System Under Unbalanced Grid Conditions," *IEEE Trans. Power Electron.*, vol. 27, no. 12, pp. 4858 - 4867, Dec. 2012.

[6] Q. Tu, Z. Xu, "Impact of Sampling Frequency on Harmonic Distortion for Modular Multilevel Converter," *IEEE Trans. Power Del.*, vol. 26, no. 1, pp. 298-306, Jan. 2011.

[7] M. Vasiladiotis, N. Cherix and A. Rufer, "Accurate Capacitor Voltage Ripple Estimation and Current Control Considerations for Grid-Connected Modular Multilevel Converters," *IEEE Trans. Power Electron.*, vol. 29, no. 9, pp. 4568-4579, Sep. 2014.

[8] B. Li, Z. Xu, S. Shi, D. Xu and W. Wang, "Comparative Study of the Active and Passive Circulating Current Suppression Methods for Modular Multilevel Converters," *IEEE Trans. Power Electron.*, vol. 33, no. 3, pp. 1878-1883, Mar. 2018.

[9] K. Wang, Y. Li, Z. Zheng and L. Xu, "Voltage Balancing and Fluctuation-Suppression Methods of Floating Capacitors in a New Modular Multilevel Converter," *IEEE Trans. Ind. Electron.*, vol. 60, no. 5, pp. 1943-1954, May. 2013.

[10] G. P. Adam, I. A. Abdelsalam, and K. H. Ahmed, et al., "Hybrid Multilevel Converter with Cascaded H-bridge Cells for HVDC Applications: Operating Principle and Scalability," *IEEE Trans. Power Electron.*, vol. 30, no. 1, pp. 65-77, Jan. 2015.

[11] G. P. Adam, K. H. Ahmed and B. W. Williams, "Mixed cells modular multilevel converters," in *Proc. IEEE ISIE*, Istanbul, Turkey, Jun. 1-4, 2014, pp. 1390-1395.

[12] J. Hu, M. Xiang, L. Lin, et al., "Improved Design and Control of FBSM MMC with Boosted AC Voltage and Reduced DC Capacitance," *IEEE Trans. Ind. Electron.*, vol. 65, no. 3, pp. 1919-1930, Mar. 2018.

[13] R. Zeng, L. Xu, L. Yao and B. W. Williams, "Design and Operation of a Hybrid Modular Multilevel Converter," *IEEE Trans. Power Electron.*, vol. 30, no. 3, pp. 1137-1146, Mar. 2015.

[14] P. D. Judge, G. Chaffey, M. M. C. Merlin, et al., "Dimensioning and Modulation Index Selection for the Hybrid Modular Multilevel Converter," *IEEE Trans. Power Electron.*, vol. 33, no. 5, pp. 3837-3851, May. 2018.

[15] W. Lin, D. Jovcic, S. Nguefeu and H. Saad, "Full-Bridge MMC Converter Optimal Design to HVDC Operational Requirements," *IEEE Trans. Power Del.*, vol. 31, no. 3, pp. 1342-1350, Jun. 2016.

[16] Y. Luo, Z. Li, L. Xu, X. Xiong, Y. Li and C. Zhao, "An Adaptive Voltage-Balancing Method for High-Power Modular Multilevel Converters," *IEEE Trans. Power Electron.*, vol. 33, no. 4, pp. 2901-2912, April 2018.

[17] K. Ilves, S. Norrga, L. Harnefors, H. P. Nee, "On energy storage requirements in modular multilevel converters", *IEEE Trans. Power Electron.*, vol. 29, no. 1, pp. 77-88, Jan. 2014.

[18] Q. Tu, Z. Xu and L. Xu, "Reduced Switching-Frequency Modulation and Circulating Current Suppression for Modular Multilevel Converters," *IEEE Trans. Power Del.*, vol. 26, no. 3, pp. 2009-2017, July. 2011.

[19] R. Li, J. E. Fletcher and B. W. Williams, "Influence of third harmonic injection on modular multilevel converter-based high-voltage direct current transmission systems," *IET Gen. Transm. Distrib.*, vol. 10, no. 11, pp. 2764-2770, July. 2016.

[20] A. J. Korn, M. Winkelnkemper and P. Steimer, "Low output frequency operation of the modular multi-level converter," in *Proc. IEEE ECCE*, Atlanta, GA, USA, Sep. 12-16, 2010, pp. 3993-3997.

[21] J. Pou, S. Ceballos, G. Konstantinou, et al., "Circulating Current Injection Methods Based on Instantaneous Information for the Modular Multilevel Converter," *IEEE Trans. Ind. Electron.*, vol. 62, no. 2, pp. 777-788, Feb. 2015.

[22] B. Li, Y. Zhang, G. Wang, et al., "A Modified Modular Multilevel Converter With Reduced Capacitor Voltage Fluctuation," *IEEE Trans. Ind. Electron.*, vol. 62, no. 10, pp. 6108-6119, Oct. 2015.

[23] M. Huang and J. Zou and X. Ma, "Hybrid Modular Multilevel Converter with Redistributed Power to Reduce Sub-Module Capacitor Voltage Fluctuation," *IEEE Trans. Power Electron.*, vol. 33, no. 8, pp. 6595-6607, Aug. 2018.

[24] Y. Lyu, C. Li, Y. Hsieh, et al., "Capacitor voltage ripple reduction with state trajectory analysis for modular multilevel converter," in *Proc. IEEE APEC*, Tampa, FL, USA, Mar. 26-30, 2017, pp. 1829-1836.

[25] P. Dong, J. Lyu and X. Cai, "Optimized Design and Control for Hybrid MMC With Reduced Capacitance Requirements," *IEEE Access*, vol. 6, no. 8, pp. 51069-51083, 2018.

[26] M. Lu, J. Hu, R. Zeng, W. Li and L. Lin, "Imbalance Mechanism and Balanced Control of Capacitor Voltage for a Hybrid Modular Multilevel Converter," *IEEE Trans. Power Electron.*, vol. 33, no. 7, pp. 5686-5696, Jul. 2018.

[27] L. Lin, Y. Lin, C. Xu and Y. Chen, "Comprehensive Analysis of Capacitor Voltage Fluctuation and Capacitance Design for Sub-modules in Hybrid Modular Multilevel Converter with Boosted Modulation Index," *IEEE J. Emerg. Sel. Topics Power Electron.* vol. 7, no. 4, pp. 2369-2383, Dec. 2019.

[28] P. S. Jones and C. C. Davidson, "Calculation of power losses for MMC-based VSC HVDC stations," in *Proc. IEEE EPE*, Lille, France, Sep. 2-6, 2013, pp. 1-10.

Appendix

The instantaneous power of the arm can be expressed as:

$$s_{ua\_inj} = u_{ua\_inj} \times i_{ua\_inj}$$

$$= \frac{1}{2}U_{dc}\left(1 - m\sin(\omega t) - k_3\sin(3\omega t + \varphi_3)\right) \times \frac{1}{3}I_{dc}(1 + \frac{2}{m\cos\varphi}\sin(\omega t - \varphi) + k_2\sin(2\omega t + \varphi_2))$$

$$= \frac{U_{dc}I_{dc}}{6m\cos\varphi}\left(1 - m\sin(\omega t) - k_3\sin(3\omega t + \varphi_3)\right) \times (m\cos\varphi + 2\sin(\omega t - \varphi) + k_2 m\cos\varphi\sin(2\omega t + \varphi_2))$$

$$= \frac{U_{dc}I_{dc}}{6m\cos\varphi}\left(\begin{array}{l} m\cos\varphi - m^2\cos\varphi\sin(\omega t) - k_3 m\cos\varphi\sin(3\omega t + \varphi_3) + 2\sin(\omega t - \varphi) - 2m\sin(\omega t)\sin(\omega t - \varphi) - 2k_3\sin(\omega t - \varphi)\sin(3\omega t + \varphi_3) \\ +k_2 m\cos\varphi\sin(2\omega t + \varphi_2) - k_2 m^2\cos\varphi\sin(\omega t)\sin(2\omega t + \varphi_2) - k_2 k_3 m\cos\varphi\sin(3\omega t + \varphi_3)\sin(2\omega t + \varphi_2) \end{array}\right)$$

$$= \frac{U_{dc}I_{dc}}{6m\cos\varphi}\left(\begin{array}{l} m\cos\varphi - m^2\cos\varphi\sin(\omega t) - k_3 m\cos\varphi\sin(3\omega t + \varphi_3) + 2\sin(\omega t - \varphi) - 2m\sin(\omega t)\sin(\omega t - \varphi) + k_2 m\cos\varphi\sin(2\omega t + \varphi_2) \\ +m\left[\sin(2\omega t - \varphi) - \cos\varphi\right] + k_3\left[\cos(4\omega t + \varphi_3 - \varphi) - \cos(2\omega t + \varphi_3 + \varphi)\right] \\ +\frac{1}{2}k_2 m^2\cos\varphi\left[\cos(3\omega t + \varphi_2) - \cos(\omega t + \varphi_2)\right] + \frac{1}{2}k_2 k_3 m\cos\varphi\left[\cos(5\omega t + \varphi_3 + \varphi_2) - \cos(\omega t + \varphi_3 - \varphi_2)\right] \end{array}\right)$$

By combining the similar terms, the expressions of harmonics can be obtained:

$$\begin{cases} s_{ua\_inj\_0} = 0 \\ s_{ua\_inj\_1} = \frac{I_{dc}U_{dc}}{12m\cos\varphi}\left[-k_2 k_3 m\cos\varphi\cos(\omega t - \varphi_2 + \varphi_3) - k_2 m^2\cos\varphi\cos(\omega t + \varphi_2) - 2m^2\sin(\omega t)\cos\varphi + 4\sin(\omega t - \varphi)\right] \\ s_{ua\_inj\_2} = \frac{I_{dc}U_{dc}}{6m\cos\varphi}\left[k_2 m\cos\varphi\sin(2\omega t + \varphi_2) - k_3\cos(2\omega t + \varphi + \varphi_3) + m\cos(2\omega t - \varphi)\right] \\ s_{ua\_inj\_3} = \frac{I_{dc}U_{dc}}{6m\cos\varphi}\left[-k_3 m\sin(3\omega t + \varphi_3)\cos\varphi + \frac{1}{2}k_2 m^2\cos\varphi\cos(3\omega t + \varphi_2)\right] \\ s_{ua\_inj\_4} = \frac{I_{dc}U_{dc}}{6m\cos\varphi}k_3\cos(4\omega t - \varphi + \varphi_3) \\ s_{ua\_inj\_5} = \frac{I_{dc}U_{dc}}{12m\cos\varphi}mk_2 k_3\cos\varphi\cos(5\omega t + \varphi_2 + \varphi_3) \end{cases}$$

Jianzhong Xu (M'14-SM'19) was born in Shanxi, China. He received the B.S. and Ph.D. degrees from North China Electric Power University (NCEPU) in 2009 and 2014 respectively. Currently, he is an Associate Professor and Ph.D. Supervisor of the State Key Laboratory of Alternate Electrical Power System with Renewable Energy Sources, North China Electric Power University, China, where he obtained his Ph.D. degree in 2014. From 2012 to 2013 and 2016 to 2017, he was a visiting Ph.D. student and Post-Doctoral Fellow at the University of Manitoba, Canada. He is an Associate Editor of the CSEE Journal of Power and Energy Systems. He is now working on the Electromagnetic Transient (EMT) equivalent modelling, fault analysis and protection of HVDC Grids.

Weicheng Deng was born in Jiangxi, China. he received the B.S. degree in power system and its automation from North China Electric Power University (NCEPU) in 2019, where he is currently working toward her master degree. His research interests include HVdc grid operation and protection.

Chenxiang Gao was born in Shanxi, China. He received the B.S. degrees in the power system and its automation from North China Electric Power University (NCEPU) in 2019. Currently, he is working towards the master degree with NCEPU. His research interests include the electromagnetic transient (EMT) equivalent modelling of MMC-HVDC and power electronic transformers (PET) in DC Grid.

Feng Lu was born in Zhejiang, China. he received the B.S. and M.S. degree in power system and its automation from North China Electric Power University (NCEPU) in 2017 and 2020. Currently, he is working in Zhejiang Wenzhou Power Supply Company. His research interests include HVdc grid operation and protection.

Jun Liang (M'02-SM'12) received the B.Sc. degree in Electric Power System & its Automation from Huazhong University of Science and Technology, Wuhan, China, in 1992 and the M.Sc. and Ph.D. degrees in Electric Power System & its Automation from the China Electric Power Research Institute (CEPRI), Beijing, in 1995 and 1998, respectively.

From 1998 to 2001, he was a Senior Engineer with CEPRI. From 2001 to 2005, he was a Research Associate with Imperial College London, U.K. From 2005 to 2007, he was with the University of Glamorgan as a Senior Lecturer. He is currently a Professor in Power Electronics with the School of Engineering, Cardiff University, Cardiff, U.K. He is the Coordinator and Scientist-in-Charge of two European Commission Marie-Curie Action ITN/ETN projects: MEDOW (€3.9M) and InnoDC (€3.9M). His research interests include HVDC, MVDC, FACTS, power system stability control, power electronics, and renewable power generation.

Prof. Liang is a Fellow of the Institution of Engineering and Technology (IET). He is the Chair of IEEE UK and Ireland Power Electronics Chapter. He is an Editorial Board Member of CSEE JPES. He is an Editor of the IEEE Transactions on Sustainable Energy.

Chengyong Zhao (M'05-SM'15) was born in Zhejiang, China. He received the B.S., M.S. and Ph.D. degrees in power system and its automation from NCEPU in 1988, 1993 and 2001, respectively. He was a visiting professor at the University of Manitoba from Jan. 2013 to Apr. 2013 and Sep. 2016 to Oct. 2016. Currently, he is a professor at the School of Electrical and Electronic Engineering, NCEPU. His research interests include HVDC system and DC grid.

Gen Li (M'18) received the B.Eng. degree in Electrical Engineering and its Automation from Northeast Electric Power University, Jilin, China, in 2011, the M.Sc. degree in Power Engineering from Nanyang Technological University, Singapore, in 2013 and the Ph.D. degree in Electrical Engineering from Cardiff University, Cardiff, U.K., in 2018.

From 2013 to 2016, he was a Marie Curie Early Stage Research Fellow funded by the European Union's MEDOW project. He has been a Visiting Researcher at China Electric Power Research Institute and Global Energy Interconnection Research Institute, Beijing, China, at Elia, Brussels, Belgium and at Toshiba International (Europe), London, U.K. He has been a Research Associate at the School of Engineering, Cardiff University since 2017. His research interests include control and protection of HVDC and MVDC technologies, power electronics, reliability modelling and evaluation of power electronics systems.

Dr. Li is a Chartered Engineer in the U.K. He is an Associate Editor of the CSEE Journal of Power and Energy Systems. He is an Editorial board member of CIGRE ELECTRA. His Ph.D. thesis received the First CIGRE Thesis Award in 2018.